










# Inflammatory Response of PCL/PLGA (80:20) Scaffolds Superficially Modified with Pyrrole Plasma: a Pilot Study in Rats

Julio César Sánchez-Pech<sup>1</sup>, Raúl Rosales-Ibáñez<sup>2</sup>, Jesus Giovanni Rodríguez-Martínez<sup>2</sup>, Alonso Reyes-Matute<sup>3</sup>, María Leticia Olga Flores-Sánchez<sup>4</sup>, José Manuel Cervantes-Uc<sup>5</sup>, Gaspar Eduardo Martín-Pat<sup>5</sup>, Andrés Iván Oliva Arias<sup>6</sup>, Cristian Carrera Figueiras<sup>1</sup>, Alejandro Ávila-Ortega<sup>1,\*</sup>

<sup>1</sup> Facultad de Ingeniería Química, Universidad Autónoma de Yucatán, Mérida, Yucatán, México; [jcsanchezpech@gmail.com](mailto:jcsanchezpech@gmail.com) (J.C.S.-P.); [cristian.carrera@correo.uady.mx](mailto:cristian.carrera@correo.uady.mx) (C.C.F.); [alejandro.avila@correo.uady.mx](mailto:alejandro.avila@correo.uady.mx) (A.A.-O.);

<sup>2</sup> Laboratorio de Ingeniería Tisular y Medicina Traslacional, Clínica Cuauhtec, Universidad Nacional Autónoma de México, Ciudad de México, México; [rosales\\_ibanez@unam.mx](mailto:rosales_ibanez@unam.mx) (R.R.-I.); [jesusjiovanni@outlook.com](mailto:jesusjiovanni@outlook.com) (J.J.R.-M.);

<sup>3</sup> Facultad de Medicina Veterinaria y Zootecnia, Departamento de Patología, Universidad Nacional Autónoma de México, Ciudad de México, México; [armatute@fmvz.unam.mx](mailto:armatute@fmvz.unam.mx);

<sup>4</sup> Universidad Nacional Autónoma de México, Bioterio de la Facultad de Estudios Superiores Iztacala, Estado de México, México; [mlflores@unam.mx](mailto:mlflores@unam.mx);

<sup>5</sup> Centro de Investigación Científica de Yucatán, Yucatán, A.C., Unidad de Materiales, Mérida, Yucatán, México; [manuelcervantes0810@gmail.com](mailto:manuelcervantes0810@gmail.com) (J.M.C.-U.); [duardoe.6p4@gmail.com](mailto:duardoe.6p4@gmail.com) (G.E.M.-P.);

<sup>6</sup> CINVESTAV del IPN Unidad Mérida, Departamento de Física Aplicada, Mérida, Yucatán, México; [andresivanolivaarias@gmail.com](mailto:andresivanolivaarias@gmail.com);

\* Correspondence: [alejandro.avila@correo.uady.mx](mailto:alejandro.avila@correo.uady.mx) (A.A.-O.);

Scopus Author ID 56002660100

Received: 25.11.2023; Accepted: 28.01.2024; Published: 10.12.2024

**Abstract:** The assessment of inflammation induced by a scaffold is vital in tissue engineering, as these studies help determine if acute inflammation can progress to chronic inflammation, exacerbating conditions such as diabetic wounds or even cancer. This study describes the methodology for manufacturing a PCL/PLGA (80:20) scaffold treated superficially with pyrrole plasma. The objective of the superficial treatment was to deposit bonds such as N-H, C=C, and C=N on the polymer surface, previously suggested in the literature for their potential to regulate the inflammatory response. FTIR and XPS analyses confirmed the presence of these bonds on the scaffold's surface. Additionally, SEM micrographs of the scaffold revealed the presence of defect-free fibers with diameters between 1 and 6  $\mu\text{m}$  and the deposition of polymeric particles derived from pyrrole. To assess the inflammatory response induced by the superficially treated scaffolds, cytotoxicity studies were initially conducted using MTT with Human Dental Follicle Stem Cells (hDFSCs), revealing no cytotoxic effects. Subsequently, the scaffolds were implanted subcutaneously *in vivo* in Wistar rats. Histological analyses of the biopsies demonstrated the expected inflammatory response to a foreign body, suggesting that the scaffolds can be considered biocompatible. These findings are relevant for the future development of surface-modified biomaterials.

**Keywords:** PCL/PLGA (80/20) scaffolds; surface treatment; pyrrole plasma; *in vivo* and *in vitro* assay; inflammatory response.

© 2024 by the authors. This article is an open-access article distributed under the terms and conditions of the Creative Commons Attribution (CC BY) license (<https://creativecommons.org/licenses/by/4.0/>).

## 1. Introduction

In tissue engineering, biomaterials or scaffolds are considered foreign bodies when implanted. Therefore, it is crucial to consider the factors that could trigger inflammation during their design or manufacturing [1,2]. The implantation of biomaterials or scaffolds triggers an acute inflammatory response, which, if not properly regulated, can progress to chronic inflammation, predisposing to long-term diseases such as diabetes, wounds, osteoarthritis, and even cancer [3-5].

The electrospinning process has been extensively applied and documented due to its versatility for manufacturing scaffolds composed of fibers [6-8]. These scaffolds can stimulate regeneration processes by mimicking the extracellular matrix. Moreover, the morphology of the fibers, their diameter, and the size of the pores play a crucial role in enhancing the regenerative process when implanted in vivo [9]. One of the scaffolds reported in the literature is obtained from a mixture of PCL/PLGA (80/20), widely utilized in tissue regeneration due to its advantageous potential balance between mechanical and biological properties. Additionally, this scaffold produces minimal inflammatory effects [10-14].

Inflammatory reactions can vary depending on the presence of various functional groups or chemical bonds. Literature reports indicate that the NH<sub>2</sub> functional group enhances the secretion of pro-inflammatory markers and the recruitment of macrophages during the acute inflammation process [15]. Zimmermann-Franco et al. [16] investigated the effect of imines (C=N) in vitro, concluding that this compound exhibits low cytotoxicity; furthermore, their in vivo results, obtained through studies conducted in mice, also indicate that it displays an anti-inflammatory profile. In another study conducted by Zaragoza et al. [17], it was demonstrated that the C=C bond also possesses anti-inflammatory properties, as it shows a significant effect as a cytokine suppressor. Additionally, various research studies demonstrate that the methyl group and ester bond (R-COOR') present in different compounds are associated with anti-inflammatory properties and wound healing [18-20].

Based on the above, using surface-modified electrospun scaffolds to incorporate functional groups can be considered an alternative for regulating inflammation. This approach offers the advantage of preserving the scaffold's mechanical and biological properties.

Various techniques and strategies can be employed to modify the surface of a scaffold, including wet chemistry methods, chemical crosslinking with crosslinking agents, chemical functionalization with different bonds, and plasma treatment [21,22]. Plasma treatment, in particular, offers the advantage of preserving the scaffold's physical properties, such as modulus of elasticity and deformation at the breaking point. Additionally, it is considered a clean treatment that only requires monomers, thereby minimizing the risk of cytotoxicity as it does not involve solvents or other precursors. Polypyrrole is one of the monomers most commonly synthesized by plasma for tissue engineering applications, primarily due to its demonstrated ability to enhance cell proliferation and biocompatibility [23-26]. Interestingly, when this monomer comes into contact with the plasma, its chemical structure breaks, and bonds such as N-H, C=N, and C=C, among others, can be deposited on the surface of biomaterials [27]. As mentioned earlier, these bonds play a positive role in the inflammatory process.

This study describes the methodology employed for fabricating an electrospun scaffold made from a blend of PCL/PLGA (80/20) superficially modified with pyrrole plasma. To evaluate the in vivo inflammatory response of the treated scaffold, MTT assays were first

conducted to verify its cytotoxicity using hDFSCs. Subsequently, after confirming the scaffold's non-cytotoxicity, it was subcutaneously implanted into the backs of 9 Wistar rats for 2, 12, and 30 days. Biopsies were then extracted for histological analysis.

The innovation of this research lies in the deposition of bonds such as N-H, C=C, and C=N on the surface of PCL/PLGA scaffolds and their practical evaluation to determine their effect on the inflammatory response. Histological findings, showing a controlled inflammatory response and the absence of cytotoxic effects, indicate that the treated scaffolds may be a viable option for tissue engineering applications. These results open up new possibilities for the development of surface-modified biomaterials.

## 2. Materials and Methods

### 2.1. *Obtention of PCL/PLGA (80/20) scaffolds and Plasma treatment.*

The electrospinning of the PCL/PLGA (80/20) scaffold and its subsequent superficial treatment was conducted according to the methodology reported previously with some modifications [11], where PCL with  $M_w = 80,000$  g/mol,  $T_m = 58^\circ\text{C}$ - $60^\circ\text{C}$ , and  $T_g = -60^\circ\text{C}$  (Sigma-Aldrich, USA); and PLGA with 75:25 (lactic: glycolic) ratio,  $M_w = 76000$ g/mol, and  $T_g = 49^\circ\text{C}$ - $55^\circ\text{C}$  (Sigma-Aldrich, USA) was used for the scaffolds fabrication. A polymer mixture of PCL/PLGA (80:20 w/w) was dissolved in a solvent mixture of trichloromethane/ethanol (10:1 v/v) (Fermont, México) at a concentration of 13% w/v. The polymeric solution was stirred for 4 h at  $25^\circ\text{C}$ . For the scaffold manufacture, an electrospinning equipment (NABOND TL-01, China) was used. During the process, 8 kV was applied to the polymeric solution, the distance between the capillary (8G) and the collector was kept at 11 cm, and a flow of 2 ml/h was maintained. The resulting samples were designated as PCL/PLGA.

The surface treatment of PCL/PLGA scaffolds with pyrrole (Sigma-Aldrich, USA) plasma was performed in a reactor coupled to a 13.56 Hz radiofrequency power supply (Advance Energy, USA). The electrospun scaffolds were cut into 2 cm x 2 cm squares to be placed in the reactor chamber. The scaffold samples were treated for 15 min at 15 W by using 9 cm between electrodes and a vacuum pressure of  $5 \times 10^{-2}$  Torr -  $9 \times 10^{-2}$  Torr. The resulting samples were designated as PCL/PLGA/PPy.

### 2.2. *Physicochemical characterization.*

#### 2.2.1. Scanning electron microscopy (SEM).

The analysis of the changes in the surface morphology of the PCL/PLGA and PCL/PLGA/PPy scaffolds was examined by scanning electron microscopy (SEM) using a JEOL JSM6369LV (Japan) equipment after coating the surfaces with a thin gold layer for better electroconductivity. The obtained micrographs were divided into four quadrants, and the diameters of the fibers, pore diameter, and particle size of PPy deposited on the scaffold surface were measured ( $n = 100$ ) for statistical purposes using the free software Image-J.

#### 2.2.2. Fourier transform infrared (FTIR) analysis.

The FTIR analysis from PCL/PLGA and PCL/PLGA/PPy scaffolds was performed with Nicolet 8700 equipment (Thermo Scientific, USA), using attenuated total reflectance

(FTIR-ATR) mode with a Ge crystal in the 4000  $\text{cm}^{-1}$ -650  $\text{cm}^{-1}$  wave number range, analyzing a total of 100 scans and a resolution of 4  $\text{cm}^{-1}$ .

### 2.2.3. X-ray photoelectron spectroscopy (XPS).

XPS spectra were obtained from PCL/PLGA and PCL/PLGA/PPy scaffolds, using ESCA/SAM equipment, model 560 (K-Alpha, Thermo Scientific, Waltham, MA, USA) with radiation of  $\text{AlK}\alpha$  at 600 W and an analysis angle of 50°. Wide-range spectra were recorded using 100 eV and 1 eV steps. High-resolution spectra of O1s, C1s, and N1s regions were recorded using 50 eV pass energy and 0.1 eV step. Deconvoluted functions (Gaussian) were realized with the OriginPro 2018 software.

## 2.3. Biological characterization.

### 2.3.1. Evaluation of cytotoxicity.

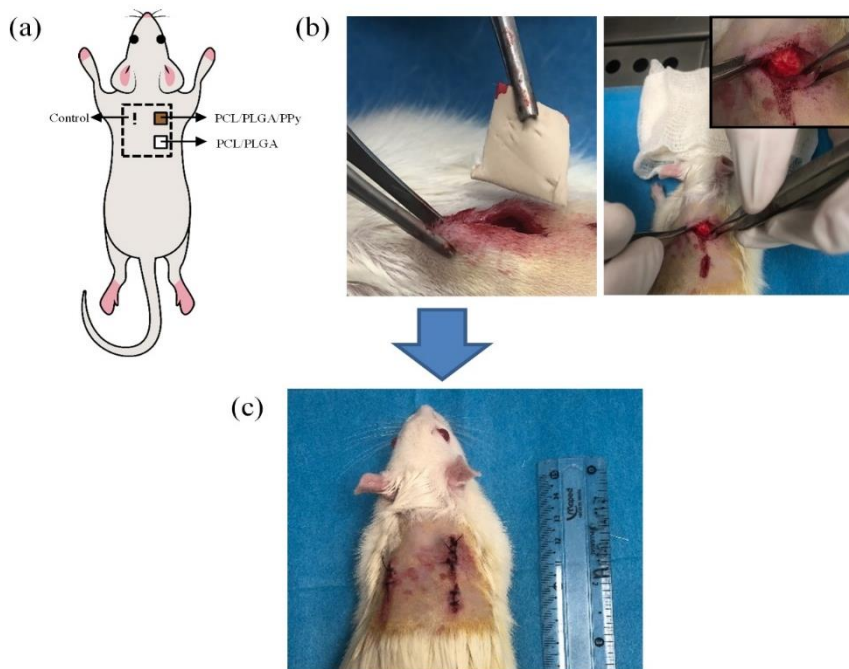
Before the MTT assays, sections of the scaffolds ( $\phi = 5$  mm) were placed in 96-well flat-bottom culture plates (Thermo Scientific Nunc) and subjected to UV radiation for 20 min on each side to sterilize the samples. Human dental follicle stem cells (hDFSCs) were donated by the Laboratorio de Ingeniería Tisular y Medicina Traslacional, Clínica Cuauhtepac, Universidad Nacional Autónoma de México (UNAM), Mexico City. The hDFSC ( $10 \times 10^3$ ) were incubated in contact with the PCL/PLGA and PCL/PLGA/PPy scaffolds for 3, 7, and 10 days at 37°C, 5%  $\text{CO}_2$ , and 95% oxygen, five replicates per each sample were used for the biological evaluation. Cell proliferation was measured by reducing tetrazolium salts to formazan with MTT (Roche Life Science; Indianapolis, USA). After each time, 100  $\mu\text{l}$  of 10% MTT reagent was placed in each well. The culture plate was placed in the incubator for 4 h, and then 100  $\mu\text{l}$  of isopropanol was added to each well to solubilize the formazan salts. The culture plate was placed back in the incubator at 37°C with 5%  $\text{CO}_2$ , and after 12 h, the readings were carried out using a microplate reader (PKL PPC142, Pokler Italy), using a wavelength of 570 nm. The significant difference between the control and scaffolds was statistically analyzed by Student's t-test in Microsoft Excel ( $p < 0.05$ ).

### 2.3.2. In vivo evaluation and histological analysis.

All procedures performed on animals were carried out by the standard NOM 062 ZOO 1999, "Technical specifications for the production, care, and use of laboratory animals". For implantation in subcutaneous skin, 9 female Wistar rats with 3-month-old were used and divided into three groups based on the sample collection period. Each specimen weighed 235 g and was housed in the Animal Facility at the Facultad de Estudios Superiores, UNAM, State of Mexico, Mexico.

For the surgical procedure, the rats received an injection with intraperitoneal anesthesia at a dose of 40 mg/kg (BW) of Ketamine (CHEMINOVA, REG SAGARPA Q-7048030) and 5mg/kg (BW) of Xylazine (PISA REG SAGARPA Q -7833-099).

Before surgery, the surgical area in the dorsal region of each rat was cleaned and disinfected with an iodine solution. Subsequently, three 1 cm incisions were made using sterile scalpel blade No. 15; scaffolds previously sterilized by UV for 1 h were placed in two incisions. The implants were made in the subcutaneous tissue, as shown in Figure 1. Finally, the incisions were sutured with a 3-0 poly(glycolic acid) thread with a simple stitch.



**Figure 1.** (a) Diagram of the animal model showing the implant zones; (b) scaffold implant; (c) Sutured tissue.

With the scaffolds implanted, 5 mg/kg (BW) of enrofloxacin was administered to each rat (Senosiain SAGARPA Q-6066-007) as antibiotic therapy. The rats were placed in their respective housing, with free access to food and water. Once the evaluation times (2, 12, and 30 days) were completed, the specimens were euthanized with an overdose of CO<sub>2</sub>.

Skin biopsies were fixed in 10% buffered formalin for 24 h. Then, two cuts in the central area of the skin fragments (related to subcutaneous swelling) were made. These samples were embedded in paraffin blocks, and sections of 4 μm were formed. Preparations were stained using the standard hematoxylin-eosin method and evaluated using light microscopy.

### 3. Results and Discussion

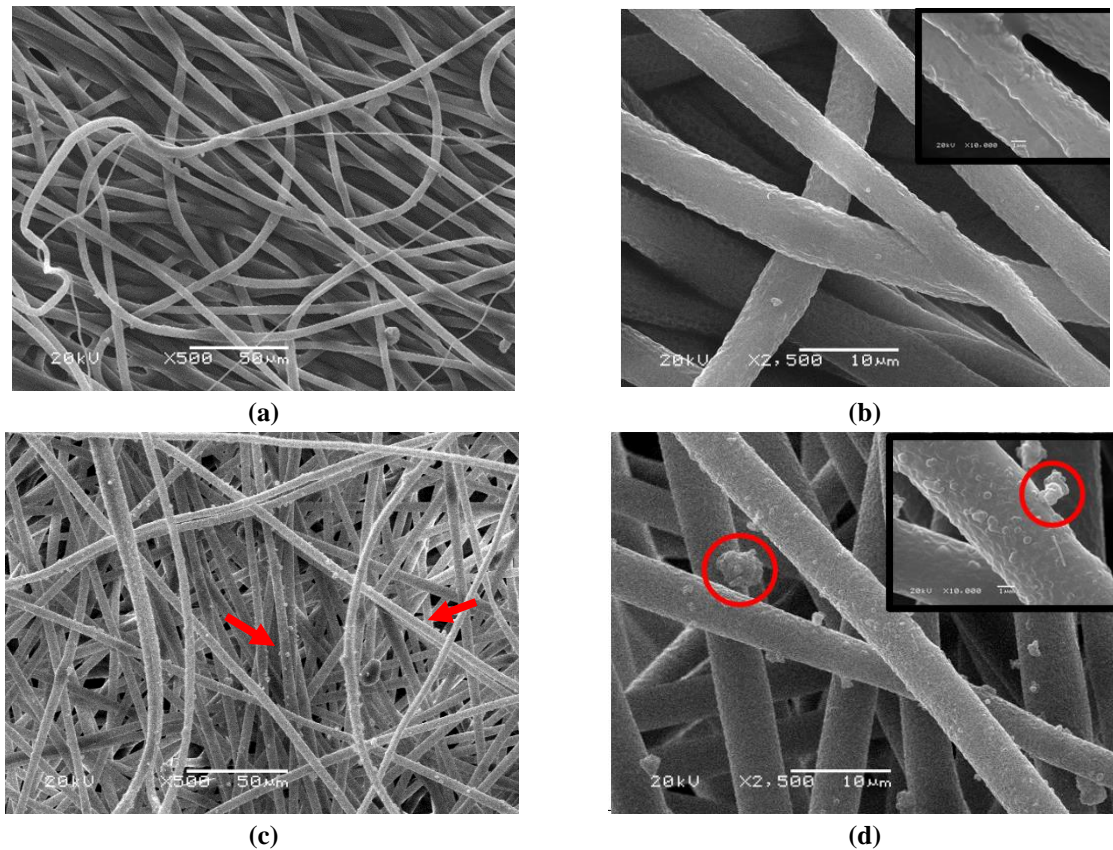
#### 3.1. Scanning electron microscopy.

SEM micrographs in Figure 2a show the microstructure of the scaffolds. As can be seen, the scaffold shows defect-free fibers with diameters between 1 and 6 μm; pore measurements in the overlapping fibers showed an average value of  $11.32 \pm 2.24$  μm. A study by Fioretta et al. [28] reported that these fibers and pore sizes promote smooth muscle cell adhesion and filtration. In another study, Horst et al. [29] reported the cell growth of smooth muscle cells in PLGA scaffolds with fiber diameter between 4.67 μm and 4.80 μm, with good cell adhesion and filtration. Thus, fiber size and pore diameter on the micrometric scale favor the transfer of nutrients and oxygen to the cells. Therefore, they are critical variables for tissue regeneration.

Higher magnification of SEM micrographs, as shown in Figure 2b, also indicates that fibers exhibit roughness. A few studies have proposed that fiber roughness also influences cell adhesion and scaffold proliferation [30-32].

SEM micrographs in Figure 2(c-d) show the formation of PPy particles on the scaffold's surface after the plasma treatment. It has been reported that pyrrole monomers can react with the free radicals formed when the scaffold is exposed to the plasma discharge, producing PPy particle nucleation sites that can increase in size with treatment time [33]. For a treatment time of 15 min, the particles reached  $1.5 \pm 0.31$  μm diameter.

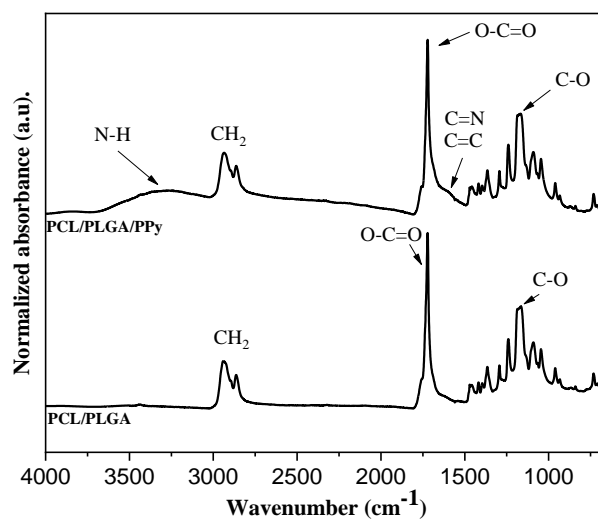




**Figure 2.** SEM micrographs of PCL/PLGA scaffolds: (a) 500X; (b) 2500X; PCL/PLGA/PPy scaffolds: (c) 500X; (d) 2500X.

### 3.2. Fourier transform infrared spectroscopy (FTIR).

Figure 3 shows the FTIR spectra of the PCL/PLGA and PCL/PLGA/PPy scaffolds, and some differences can be observed. Both spectra showed bands at  $2862\text{ cm}^{-1}$  related to  $\text{CH}_2$  groups, at  $1726\text{ cm}^{-1}$  associated with the  $\text{O-C=O}$  group, and at  $1294\text{ cm}^{-1}$  attributed to the  $\text{C-O}$ . The peaks at  $1242\text{ cm}^{-1}$  and  $1160\text{ cm}^{-1}$  correspond to the  $\text{C-O-C}$  and the  $-\text{C-O}$  bonds, respectively, associated with the functional groups of PCL and PLGA [34,35].



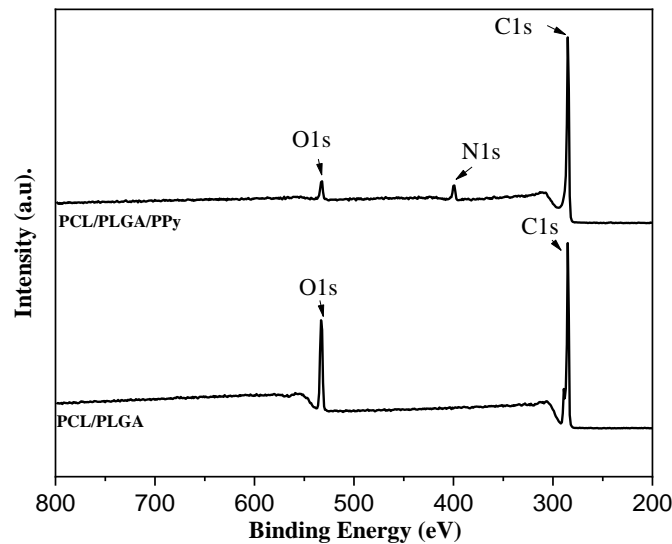
**Figure 3.** FTIR spectrum of PCL/PLGA and PCL/PLGA/PPy scaffolds.

Interestingly, the PCL/PLGA/PPy scaffold spectrum showed a broad band at  $3400\text{ cm}^{-1}$  corresponding to the N-H stretching vibration of amines. Another characteristic peak of pyrrole was found at  $1635\text{ cm}^{-1}$ , which is attributed to the  $\text{C=C}$  and  $\text{C=N}$  bonds [27].

Additionally, there is a possible contribution of the secondary N-H groups (amide II) in bending, chemically bonded to the carbonyl groups of PCL/PLGA [33], which are not observed in the sample without treatment. These results agree with those reported for PPy [36], confirming that the incorporation of PPy on the scaffold surface was successfully achieved.

### 3.3. X-ray photoelectron spectroscopy.

The XPS survey spectra of the PCL/PLGA and PCL/PLGA/PPy scaffolds are presented in Figure 4. Peaks of C1s and O1s were found at 284.8 eV and 531 eV, respectively. The spectrum of the PPy plasma-treated scaffold also showed the N1s signal at 400 eV, which is not present in the untreated scaffold; this result contributes to confirming the presence of PPy in the plasma-treated scaffold [37]. Table 1 presents the elemental quantitative analysis obtained from the XPS windows, and it is observed that the N content in the scaffolds subjected to pyrrole plasma treatment is 4.3%. As a consequence of the incorporation of polypyrrole particles, a reduction in O1s content was attained from 18.9% to 3.8 %, as well as an increase in C content from 81.1% to 91.9%. These differences in values can be attributed to the fact that during plasma treatment, the pyrrole ring breaks down, and new bonds carbon-carbon bonds are created [38].

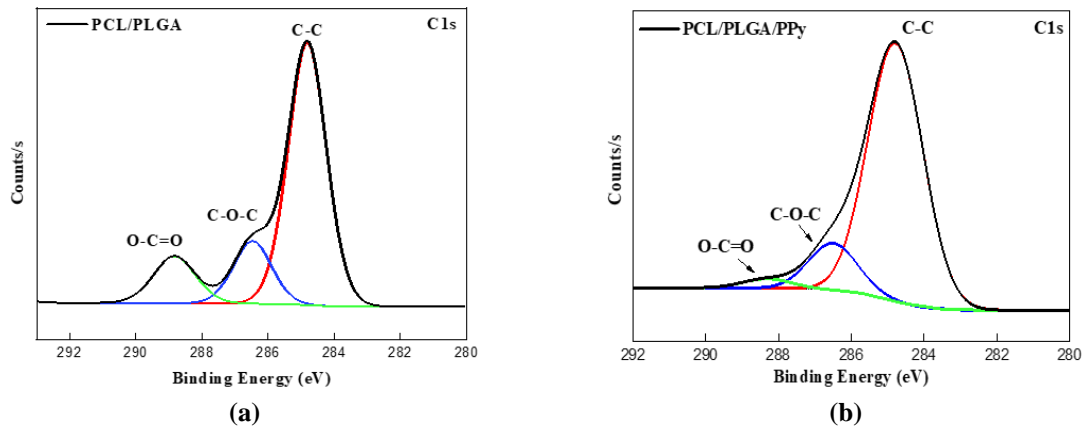


**Figure 4.** XPS survey spectra of the PCL/PLGA and PCL/PLGA/PPy scaffolds.

**Table 1.** Elemental analysis of the scaffolds.

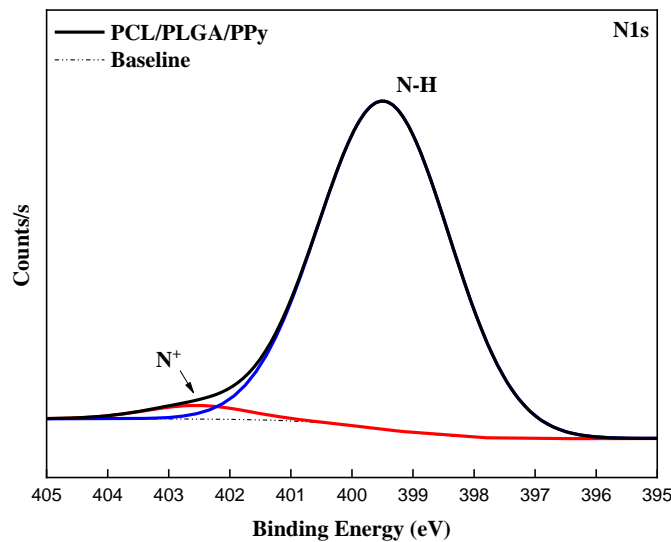
Sample	% atomic			C/N
	Carbon	Oxygen	Nitrogen	
PCL/PLGA/PPy	91.9	3.8	4.3	21.3
PCL/PLGA	81.1	18.9	0.0	---

Figure 5a shows the high-resolution spectra of the C1s signal from the PCL/PLGA scaffolds. The peak of the C-C bond is observed at 285 eV and the C-O-C bond at 286.6 eV [39]. The signal at 288.7 eV can be attributed to the O-C=O bond in the PCL and PLGA structure [40,41]. It is reported that plasma irradiation can also form free radicals evolved from the ester bonds (R-COO-R) in PCL and PLGA structures. This free radical (R-CO\*) could react with the pyrrole plasma, forming the amine bonds observed in the FTIR spectra. As a result, the peak area of the O-C=O and C-O-C bonds was depleted, as was observed in the XPS spectrum of the modified scaffold, see Figure 5b [33].



**Figure 5.** C1s spectra of the scaffolds (a) PCL/PLGA; (b) PCL/PLGA/PPy.

Figure 6 shows the deconvoluted N1s spectrum of the PCL/PLGA/PPy scaffold. The signals at 399.5 eV and 402.5 eV are attributed to the N-H groups and positively charged species N<sup>+</sup> (polaron) associated with PPy, respectively. This result agrees with the results reported by Taraballi et al. [42], who functionalized PCL with NH<sub>2</sub> groups obtaining similar spectra.



**Figure 6.** N1s spectrum of the PLGA/PCL/PPy scaffold.

### 3.4. Cytotoxicity assay.

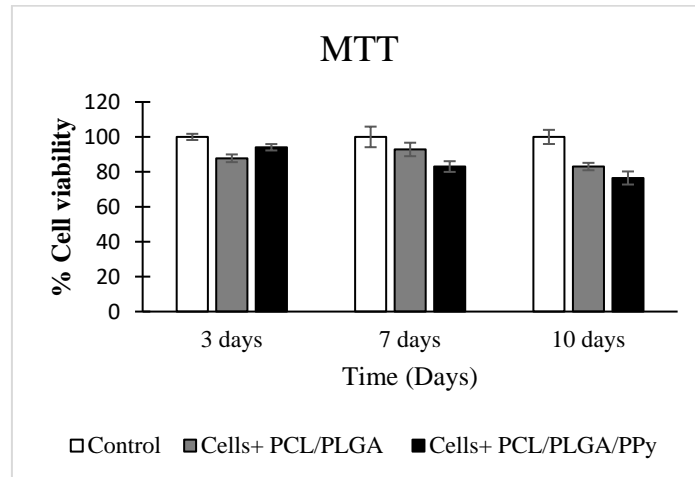
hDFSCs have been widely used in tissue engineering due to their multipotential differentiation capacity. Furthermore, they are relatively easy to obtain and come from abundant and uncontroversial sources compared with other stem cells. These features also make them suitable for use in cytotoxicity assays.

For the cytotoxicity assays, PCL/PLGA and PCL/PLGA/PPy scaffolds were placed in contact with hDFSCs for 3, 7, and 10 days. After each period, MTT assays were performed to evaluate the scaffolds' cytotoxicity. A well culture plate with dental follicle cells and culture medium was used as a control sample.

Figure 7 shows the MTT absorbance for each period. After 3 days of cell culture, the optical absorbance of the cells in contact with the PCL/PLGA scaffold was  $87.77 \pm 2.21$ ; this indicates that there was no statistically significant difference when compared to the absorbance of the PCL/PLGA/PPy scaffolds ( $94.07 \pm 1.82$ ), ( $p > 0.05$ ). After 7 days of cell culture, the PCL/PLGA and PCL/PLGA/PPy scaffolds showed absorbances of  $92.83 \pm 3.85$  and



83.03±3.03, respectively, without statistically significant difference ( $p > 0.05$ ) between them. This behavior carried on up to 10 days of cell culture; after this time, the PCL/PLGA and PCL/PLGA/PPy scaffolds showed absorbances of 83.03±2.11 and 76.49±3.73 respectively ( $p > 0.05$ ). These results indicate no statistically significant difference in cytotoxicity for the proposed times; in addition, according to ISO10993-5/12, these MTT assays indicate the non-cytotoxicity of the scaffolds since in all assays, the reduction of cell viability did not exceed 30%.



**Figure 7.** Cytotoxicity assay by 3-(4,5-dimethylthiazol-2-yl)-2,5 diphenyltetrazol (MTT) for PCL/PLGA and PCL/PLGA/PPy scaffolds. \* $p < 0.05$ .

These results are in agreement with the study reported by Li et al. [43], who performed cytotoxicity assays on PCL/PLGA scaffolds using hDFSCs; once the non-cytotoxic effect was successfully demonstrated, the authors implanted the scaffolds in vivo in Sprague-Dawley rats, obtaining favorable tissue regeneration results. On the other hand, Flores-Sánchez et al.[23] reported that a scaffold modified with pyrrole plasma showed no cytotoxicity and enhanced cell adhesion and proliferation.

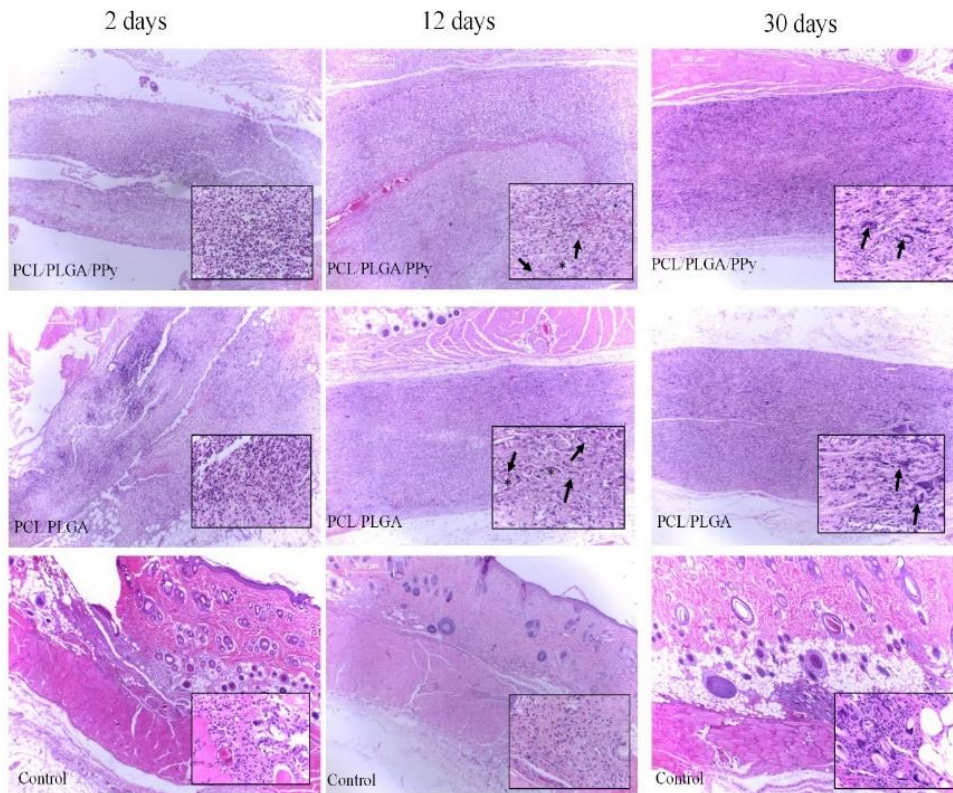
### 3.5. *In vivo* histological studies.

Various methodologies and techniques have been developed to assess the in vivo inflammatory response generated by a scaffold after implantation. This analysis can sometimes be complex and challenging to execute. A suggested initial approach is the use of subcutaneous implants in small animal models, such as rats, as several studies support the idea that these implants can provide relevant information about the inflammatory phenomena induced by the scaffold [44,45].

The skin biopsy analysis revealed an intense inflammatory response, focalized in the hypodermis, with extension to the dermis, including the cutaneous muscle in a delimited manner. The swollen tissue was a mixed infiltrate composed of predominant neutrophils and necrotic cell debris with a progression toward macrophages and multinucleated giant cells. Additionally, variable amounts of lymphocytes, plasma cells, and many scattered mast cells were identified.

Similar material was identified within the multinucleated giant cells. In some cases, foci of follicular rupture were identified, with hair exposure and associated granulomatous inflammation (furunculosis), while in other cases, sectors of ulcer, covered by scab, were identified. The scaffolds located in the center of the inflammatory lesions did not show the

staining effect and still retained their fibrous structure. Histology images are shown in Figure 8.


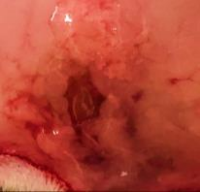
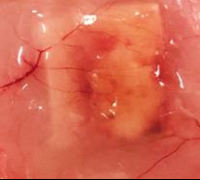
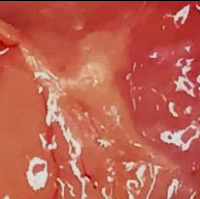


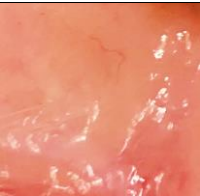
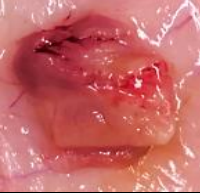



**Figure 8.** Histological analysis of the PCL/PLGA and PCL/PLGA/PPy scaffolds, where histological skin sections are observed, with focal expansion mainly of the hypodermis due to an intense inflammatory response made up of neutrophils in the initial stages (day two). On day 12, an increase in the number of macrophages and multinucleated giant cells was observed (black arrows), with the presence of intracytoplasmic foreign material compatible with the scaffolds (\*) and, later, a predominance of these last two cells (30 days). In the boxes, a close-up of the inflammatory process is observed. H&E, 40x (400x for zoomed views).

In general, a classic foreign body inflammatory response was observed in all samples, which implies the predominance of neutrophils in acute stages, with the presence of a higher proportion of necrotic tissue associated with tissue damage, followed by an increase in the number of macrophages, multinucleated giant cells, and granulation tissue. These findings revealed the presence of severe focal neutrophilic to granulomatous dermatitis associated with intralesional foreign material in both types of scaffolds, suggesting that no significant changes were observed between the inflammatory responses to both types of scaffolds (PCL/PLGA and PCL/PLGA/PPy). Additionally, it was found that the degradation rate by phagocytosis aligns with what is reported in the literature [46]. Furthermore, it is demonstrated that the inflammatory response is always expected in the presence of a foreign body, suggesting that the scaffolds can be considered biocompatible. These results are consistent with the literature, showing that PPy does not induce a severe inflammatory response [47,48]. Table 2 presents the main histological findings per case.

The PCL/PLGA scaffolds superficially treated with pyrrole plasma presented in this study could be candidates for use in tissue engineering. However, before their potential clinical application, more comprehensive investigations, such as immunohistochemistry studies and extended evaluation periods of the implanted scaffold, are required to analyze their long-term effects and determine if they induce chronic inflammation.

**Table 2.** Histological findings, where Cn represents the control sample, Tn the PCL/PLGA/PPy scaffold, and Pn the PCL/PLGA scaffold.

Representative biopsy	ID	Histological findings			
		Inflammation (predominant)	Granulation tissue	Necrosis	Foreign material (implant)
<b>2 days</b>					
	C1	lymphoplasmacytic and granulomatous	+	+++	Absent
	C2	neutrophilic	+++	+++	Absent
	C3	granulomatous	++	+	Absent
	T1	neutrophilic	++	+++	Present
	T2	neutrophilic	++	+++	Present
	T3	neutrophilic	++	+++	Present
	P1	neutrophilic	++	+++	Present
	P2	neutrophilic	++	+++	Present
	P3	neutrophilic	++	++	Present
<b>12 days</b>					
	C4	granulomatous	++	+	Absent
	C5	granulomatous	+	-	Absent
	C6	granulomatous	+	-	Absent
	T4	granulomatous	++	++	Present
	T5	granulomatous	++	++	Present
	T6	granulomatous	++	++	Present
	P4	granulomatous	++	++	Present
	P5	granulomatous	++	+	Present
	P6	granulomatous	++	+	Present
<b>30 days</b>					
	C7	granulomatous	+	-	Absent
	C8	-	+	-	Absent
	C9	granulomatous	+	-	Absent
	T7	granulomatous	++	-	Present (scarce)
	T8	granulomatous	++	-	Present (scarce)
	T9	granulomatous	++	-	Present (scarce)
	P7	granulomatous	++	-	Present (scarce)
	P8	granulomatous	++	-	Present (scarce)



<b>P9</b>	granulomatous	++	-	Present (scarce)
-----------	---------------	----	---	------------------

+, mild; ++, moderate; +++, severe and – indicate not present.

#### 4. Conclusions

The PCL/PLGA scaffolds presented fibers with diameters ranging from 1  $\mu\text{m}$  - 6  $\mu\text{m}$ . When superficially treated with pyrrole plasma, particles with globular morphology were formed on the fiber surface. These particles exhibited an average diameter size of  $1.5 \pm 0.31 \mu\text{m}$ . The results from FTIR and XPS revealed the presence of new bonds on the scaffold surface, such as N-H, C=C, and C=N, indicating that the surface treatment was successful.

MTT assays demonstrated that both modified and unmodified scaffolds are not cytotoxic. Additionally, in vivo experiments showed the expected classical inflammatory response to the presence of a foreign body. Furthermore, the scaffolds degraded through phagocytosis, suggesting their biocompatibility.

It is important to note that the surface treatment under the proposed conditions does not appear to influence the inflammatory response. Therefore, this research can be a reference for future studies on superficially modified scaffolds, exploring variables in the plasma reactor and their relationship with the inflammatory response.

#### Funding

This research received no external funding.

#### Acknowledgments

To CONAHCYT for the 'Estancias Posdoctorales por México 2021' scholarship (CVU: 510665), and to JA Lara-Arana for designing the diagram of the animal model showing the implant zones.

#### Conflicts of Interest

The authors declare no conflict of interest.

#### References

1. Lynch, R.I.; Lavelle Ed C. Immuno-modulatory biomaterials as anti-inflammatory therapeutics. *Biochem Pharmacol* **2022**, *197*, 114890, <https://doi.org/10.1016/j.bcp.2021.114890>.
2. Salthouse, D.; Novakovic, K.; Hilkens, C.M.; Ferreira, A. Interplay between biomaterials and the immune system: Challenges and opportunities in regenerative medicine. *Acta Biomater* **2023**, *155*, 1-18, <https://doi.org/10.1016/j.actbio.2022.11.003>.
3. Ye, J.; Gong, M.; Song, J.; Chen, S.; Meng, Q.; Shi, R.; Zhang, L.; Xue, J.J.P. Integrating Inflammation-Responsive Prodrug with Electrospun Nanofibers for Anti-Inflammation Application. *Pharmaceutics* **2022**, *14*, 1273, <https://doi.org/10.3390/pharmaceutics14061273>.
4. Tu, Z.; Zhong, Y.; Hu, H.; Shao, D.; Haag, R.; Schirner, M.; Lee, J.; Sullenger, B.; Leong, K. Design of therapeutic biomaterials to control inflammation. *Nat Rev Mater* **2022**, *7*, 557-574, <https://doi.org/10.1038/s41578-022-00426-z>.



5. Zahid, A.A.; Chakraborty, A.; Shamiya, Y.; Ravi, S.P.; Paul, A. Leveraging the advancements in functional biomaterials and scaffold fabrication technologies for chronic wound healing applications. *Mat. Horizon* **2022**, *9*, 1850-1865, <https://doi.org/10.1039/D2MH00115B>.
6. Mohammadalizadeh, Z.; Bahremandi-Toloue, E.; Karbasi, S. Synthetic-based blended electrospun scaffolds in tissue engineering applications. *J Mater Sci* **2022**, *57*, 4020-4079, <https://doi.org/10.1007/s10853-021-06826-w>.
7. Chen, Y.; Dong, X.; Shafiq, M.; Myles, G.; Radacsi, N.; Mo, Xiumei. Recent advancements on three-dimensional electrospun nanofiber scaffolds for tissue engineering. *Adv. Fiber Mater.* **2022**, *4*, 959-986, <https://doi.org/10.1007/s42765-022-00170-7>.
8. Flores-Rojas, G.G.; Gómez-Lazaro, B.; López-Saucedo, F.; Vera-Graziano, R.; Bucio, E.; Mendizábal, E.J.M. Electrospun Scaffolds for Tissue Engineering: A Review. *Macromolecules* **2023**, *3*, 524-553, <https://doi.org/10.3390/macromol3030031>.
9. Wang, Z.; Cui, Y.; Wang, J.; Yang, X.; Wu, Y.; Wang, K.; Gao, X.; Li, D.; Li, Y.; Zheng, X.-L.J.B. The effect of thick fibers and large pores of electrospun poly ( $\epsilon$ -caprolactone) vascular grafts on macrophage polarization and arterial regeneration. *Biomaterials* **2014**, *35*, 5700-5710, <https://doi.org/10.1016/j.biomaterials.2014.03.078>.
10. González-González, A.M.; Cruz, R.; Rosales-Ibáñez, R.; Hernández-Sánchez, F.; Carrillo-Escalante, H.J.; Rodríguez-Martínez, J.J.; Velasquillo, C.; Talamás-Lara, D.; Ludert, J.E. In Vitro and In Vivo Evaluation of a Polycaprolactone (PCL)/Polylactic-Co-Glycolic Acid (PLGA)(80: 20) Scaffold for Improved Treatment of Chondral (Cartilage) Injuries. *Polymers* **2023**, *15*, 2324, <https://doi.org/10.3390/polym15102324>.
11. Sánchez-Pech, J.C.; Rosales-Ibáñez, R.; Cauch-Rodríguez, J.V.; Carrillo-Escalante, H.J.; Rodríguez-Navarrete, A.; Avila-Ortega, A.; Hernández-Sánchez, F.J.J.o.B.A. Design, synthesis, characterization, and cytotoxicity of PCL/PLGA scaffolds through plasma treatment in the presence of pyrrole for possible use in urethral tissue engineering. *J. Biomater. Appl.* **2020**, *34*, 840-850, <https://doi.org/10.1177/0885328219882638>.
12. Rosales-Ibáñez, R.; Rodríguez-Martínez, J.; González-González, A.; Morales-de la Luz, R.; Sánchez-Pech, J.; Hernández-Sánchez, F.; Villamar-Duque, T.; González Aragón-Pineda, A.; Flores-Sánchez, M. Evaluación de la citotoxicidad de andamios de PCL y PLGA con células troncales de pulpa dental para ingeniería tisular. *Revista Internacional de Investigación e Innovación Tecnológica* **2023**, *11*, 79-94.
13. Ghafouri Azar, M.; Wiesnerova, L.; Dvorakova, J.; Chocholata, P.; Moztarzadeh, O.; Dejmeck, J.; Babuska, V.J.G. Optimizing PCL/PLGA Scaffold Biocompatibility Using Gelatin from Bovine, Porcine, and Fish Origin. *Gels* **2023**, *9*, 900, <https://doi.org/10.3390/gels9110900>.
14. Song, G.; Zhao, H.Q.; Liu, Q.; Fan, Z.J.B.M. A review on biodegradable biliary stents: materials and future trends. *Bioact Mater* **2022**, *17*, 488-495, <https://doi.org/10.1016/j.bioactmat.2022.01.017>.
15. Yin, B.; Chan, C.K.W.; Liu, S.; Hong, H.; Wong, S.H.D.; Lee, L.K.C.; Ho, L.W.C.; Zhang, L.; Leung, K.C.-F.; Choi, P.C.-L.J.A.n. Intrapulmonary cellular-level distribution of inhaled nanoparticles with defined functional groups and its correlations with protein corona and inflammatory response. *ACS Nano* **2019**, *13*, 14048-14069, <https://doi.org/10.1021/acsnano.9b06424>.
16. Zimmermann-Franco, D.C.; Esteves, B.; Lacerda, L.M.; de Oliveira Souza, I.; Dos Santos, J.A.; Pinto, N.d.C.C.; Scio, E.; da Silva, A.D.; Macedo, G. In vitro and in vivo anti-inflammatory properties of imine resveratrol analogues. *Bioorg Med Chem* **2018**, *26*, 4898-4906, <https://doi.org/10.1016/j.bmc.2018.08.029>.
17. Zaragoza, C.; Villaescusa, L.; Monserrat, J.; Zaragoza, F.; Álvarez-Mon, M.J.M. Potential therapeutic anti-inflammatory and immunomodulatory effects of dihydroflavones, flavones, and flavonols. *Molecules* **2020**, *25*, 1017, <https://doi.org/10.3390/molecules25041017>.
18. Armutcu, F.; Akyol, S.; Ustunsoy, S.; Turan, F. Therapeutic potential of caffeic acid phenethyl ester and its anti-inflammatory and immunomodulatory effects. *Exp Ther Med* **2015**, *9*, 1582-1588, <https://doi.org/10.1016/j.polymertesting.2021.107097>.
19. Toyoda, T.; Tsukamoto, T.; Takasu, S.; Shi, L.; Hirano, N.; Ban, H.; Kumagai, T.; Tatematsu, M., Anti-inflammatory effects of caffeic acid phenethyl ester (CAPE), a nuclear factor- $\kappa$ B inhibitor, on *Helicobacter pylori*-induced gastritis in Mongolian gerbils. *Int J Cancer* **2009**, *125*, 1786-1795, <https://doi.org/10.1002/ijc.24586>.
20. Orban, Z.; Mitsiades, N.; Burke Jr, T.R.; Tsokos, M.; Chrousos, G.P.J.N. Caffeic acid phenethyl ester induces leukocyte apoptosis, modulates nuclear factor-kappa B and suppresses acute inflammation. *Neuroimmunomodulation* **1999**, *7*, 99-105, <https://doi.org/10.1159/000026427>.



21. Chakraborty, R.; Anoop, A.G.; Thakur, A.; Mohanta, G.C.; Kumar, P. Strategies to Modify the Surface and Bulk Properties of 3D-Printed Solid Scaffolds for Tissue Engineering Applications. *ACS Omega* **2023**, *8*, 5139-5156, <https://doi.org/10.1021/acsomega.2c05984>.
22. Biazar, E.; Kamalvand, M.; Avani, F.; Biomaterials, P. Recent advances in surface modification of biopolymeric nanofibrous scaffolds. *Int. J. Polym. Mater. Polym. Biomater* **2022**, *71*, 493-512, <https://doi.org/10.1080/00914037.2020.1857383>.
23. Flores-Sánchez, M.G.; Islas-Arteaga, N.C.; Raya-Rivera, A.M.; Esquiliano-Rendon, D.R.; Morales-Corona, J.; Uribe-Juarez, O.E.; Vivar-Velázquez, F.I.; Ortiz-Vázquez, G.P.; Olayo, R. Effect of a plasma synthesized polypyrrole coverage on polylactic acid/hydroxyapatite scaffolds for bone tissue engineering. *J Biomed Mater Res A* **2021**, *109*, 2199-2211, <https://doi.org/10.1002/jbm.a.37205>.
24. Osorio-Londoño, D.M.; Godínez-Fernández, J.R.; Acosta-García, M.C.; Morales-Corona, J.; Olayo-González, R.; Morales-Guadarrama, A.J.P. Pyrrole plasma polymer-coated electrospun scaffolds for neural tissue engineering. *Polymers* **2021**, *13*, 3876, <https://doi.org/10.3390/polym13223876>.
25. Islas-Arteaga, N.C.; Rivera, A.R.; Rendon, D.R.E.; Morales-Corona, J.; Ontiveros-Nevarés, P.G.; Sánchez, M.G.F.; Mojica-Cardoso, C.; Olayo, R. Electrospun scaffolds with surfaces modified by plasma for regeneration of articular cartilage tissue: a pilot study in rabbit. *Int. J. Polym. Mater. Polym. Biomater.* **2019**, *68*, 1089-1098, <https://doi.org/10.1080/00914037.2018.1534109>.
26. Zhang, Z.; Roy, R.; Dugré, F.J.; Tessier, D.; Dao, L. In vitro biocompatibility study of electrically conductive polypyrrole-coated polyester fabrics. *J. Biomed. Mater. Res.* **2001**, *57*, 63-71, [https://doi.org/10.1002/1097-4636\(200110\)57:1<63::AID-JBM1142>3.0.CO;2-L](https://doi.org/10.1002/1097-4636(200110)57:1<63::AID-JBM1142>3.0.CO;2-L).
27. Wang, J.; Neoh, K.; Kang, E. Comparative study of chemically synthesized and plasma polymerized pyrrole and thiophene thin films. *Thin solid films* **2004**, *446*, 205-217, <https://doi.org/10.1016/j.tsf.2003.09.074>.
28. Fioretta, E.S.; Simonet, M.; Smits, A.I.; Baaijens, F.P.; Bouten, C. Differential response of endothelial and endothelial colony forming cells on electrospun scaffolds with distinct microfiber diameters. *Biomacromolecules* **2014**, *15*, 821-829, <https://doi.org/10.1021/bm4016418>.
29. Horst, M.; Milleret, V.; Nötzli, S.; Madduri, S.; Sulser, T.; Gobet, R.; Eberli, D., Increased porosity of electrospun hybrid scaffolds improved bladder tissue regeneration. *J Biomed Mater Res A* **2014**, *102*, 2116-2124, <https://doi.org/10.1002/jbm.a.34889>.
30. Zhou, Q.; Xie, J.; Bao, M.; Yuan, H.; Ye, Z.; Lou, X.; Zhang, Y. Engineering aligned electrospun PLLA microfibers with nano-porous surface nanotopography for modulating the responses of vascular smooth muscle cells. *J. Mater. Chem. B* **2015**, *3*, 4439-4450, <https://doi.org/10.1039/C5TB00051C>.
31. Ponsonnet, L.; Comte, V.; Othmane, A.; Lagneau, C.; Charbonnier, M.; Lissac, M.; Jaffrezic, N. Effect of surface topography and chemistry on adhesion, orientation and growth of fibroblasts on nickel-titanium substrates. *Mater Sci Eng C* **2002**, *21*, 157-165, [https://doi.org/10.1016/S0928-4931\(02\)00097-8](https://doi.org/10.1016/S0928-4931(02)00097-8).
32. Calore, A.R.; Srinivas, V.; Groenendijk, L.; Serafim, A.; Stancu, I.C.; Wilbers, A.; Leoné, N.; Sanchez, A.A.; Auhl, D.; Mota, C. Manufacturing of scaffolds with interconnected internal open porosity and surface roughness. *Acta Biomater* **2022**, *156*, 158-176, <https://doi.org/10.1016/j.actbio.2022.07.017>.
33. Martín-Pat, G.E.; Rodríguez-Fuentes, N.; Cervantes-Uc, J.M.; Rosales-Ibáñez, R.; Carrillo-Escalante, H.J.; Ku-Gonzalez, A.F.; Avila-Ortega, A.; Hernandez-Sanchez, F. Effect of different exposure times on physicochemical, mechanical and biological properties of PGS scaffolds treated with plasma of iodine-doped polypyrrole. *J Biomater Appl* **2020**, *35*, 485-499, <https://doi.org/10.1177/0885328220941466>.
34. Can-Herrera, L.; Ávila-Ortega, A.; de la Rosa-García, S.; Oliva, A.; Cauich-Rodríguez, J.; Cervantes-Uc, J. Surface modification of electrospun polycaprolactone microfibers by air plasma treatment: Effect of plasma power and treatment time. *Eur Polym J* **2016**, *84*, 502-513, <https://doi.org/10.1016/j.eurpolymj.2016.09.060>.
35. Qian, Y.; Chen, H.; Xu, Y.; Yang, J.; Zhou, X.; Zhang, F.; Gu, N. The preosteoblast response of electrospinning PLGA/PCL nanofibers: effects of biomimetic architecture and collagen I. *Int J Nanomedicine* **2016**, *11*, 4157, <https://doi.org/10.2147/IJN.S110577>.
36. Ibrahim, I.; Yunus, S.; Hashim, M. Relative performance of isopropylamine, pyrrole and pyridine as corrosion inhibitors for carbon steels in saline water at mildly elevated temperatures. *Int. J. Sci. Eng. Res.* **2013**, *4*, 1-12.
37. Tarcha, P.J.; Salvati, L.; Johnson, R. Polypyrrole Latex: Surface Analysis by XPS. *Surf. Sci. Spectra* **2001**, *8*, 312-316, <https://doi.org/10.1116/11.20020102>.
38. Li, C.; Hsieh, J.; Lee, Y.J.S.; Technology, C. Fabrication and structural characterization of plasma polymerized polypyrrole thin film. *Surf Coat Technol* **2017**, *320*, 206-212, <https://doi.org/10.1016/j.surfcoat.2017.01.049>.

39. Diller, K.; Klappenberger, F.; Allegretti, F.; Papageorgiou, A.C.; Fischer, S.; Duncan, D.A.; Maurer, R.J.; Lloyd, J.A.; Oh, S.C.; Reuter, K. Temperature-dependent templated growth of porphine thin films on the (111) facets of copper and silver. *J. Chem. Phys.* **2014**, *141*, 144703, <https://doi.org/10.1063/1.4896605>.
40. Totolin, M.; Grigoras, M. Plasma induced pyrrole polymerization. *Revue Roumaine de Chimie* **2007**, *52*, 999-1005.
41. Wan, Y.; Qu, X.; Lu, J.; Zhu, C.; Wan, L.; Yang, J.; Bei, J.; Wang, S.J.B. Characterization of surface property of poly (lactide-co-glycolide) after oxygen plasma treatment. *Biomaterials* **2004**, *25*, 4777-4783, <https://doi.org/10.1016/j.biomaterials.2003.11.051>.
42. Taraballi, F.; Zanini, S.; Lupo, C.; Panseri, S.; Cunha, C.; Riccardi, C.; Marcacci, M.; Campione, M.; Cipolla, L.J.J.o.c.; science, i. Amino and carboxyl plasma functionalization of collagen films for tissue engineering applications. *J Colloid Interface Sci* **2013**, *394*, 590-597, <https://doi.org/10.1016/j.jcis.2012.11.041>.
43. Li, X.; Yang, C.; Li, L.; Xiong, J.; Xie, L.; Yang, B.; Yu, M.; Feng, L.; Jiang, Z.; Guo, W. A therapeutic strategy for spinal cord defect: human dental follicle cells combined with aligned PCL/PLGA electrospun material. *Biomed. Res. Int.* **2015**, *2015*, 197183, <https://doi.org/10.1155/2015/197183>.
44. Gallardo, A.; Bordenave, C.; Orellano, J.; Galliano, P.; Porto Pérez, J. Evaluación de ensayos in vivo e in vitro de materiales para implantes ortopédicos: estudio preliminar. *Rev. Asoc. Arg. Ortop. y Traumatol.* **1998**, *63*, 10-17.
45. Villarreal-Gómez, L.J.; Vera-Graziano, R.; Vega-Ríos, M.R.; Pineda-Camacho, J.L.; Almanza-Reyes, H.; Mier-Maldonado, P.A.; Cornejo-Bravo, J. Biocompatibility evaluation of electrospun scaffolds of poly (L-Lactide) with pure and grafted hydroxyapatite. *J. Mex. Chem. Soc.* **2014**, *58*, 435-443.
46. Wissing, T.B.; Bonito, V.; van Haften, E.E.; van Doeselaar, M.; Brugmans, M.M.; Janssen, H.M.; Bouten, C.V.; Smits, A; Macrophage-driven biomaterial degradation depends on scaffold microarchitecture. *Front Bioeng Biotechnol* **2019**, *7*, 87, <https://doi.org/10.3389/fbioe.2019.00087>.
47. Álvarez-Mejía, L.; Salgado-Ceballos, H.; Olayo, R.; Cruz, G.; Olayo, M.; Díaz-Ruiz, A.; Ríos, C.; Mondragón-Lozano, R.; Morales-Guadarrama, A.; Sánchez-Torres, S. Efecto de implantes de polipirrol sintetizados por diferentes métodos sobre lesiones de médula espinal en ratas. *Rev. Mex. Ing. Bioméd.* **2015**, *36*, 7-21.
48. Ramanaviciene, A.; Kausaite, A.; Tautkus, S.; Ramanavicius, A; Biocompatibility of polypyrrole particles: an in-vivo study in mice. *J. Pharm. Pharmacol.* **2007**, *59*, 311-315. <https://doi.org/10.1211/jpp.59.2.0017>.